SMAR 2019 – Fifth Conference on Smart Monitoring,
Assessment and Rehabilitation of Civil Structures

SMAR 2019

Static load monitoring of a concrete bridge using a high-precision distributed fiber optic sensor system

Aleksander WOSNIOK [1], Rob JANSEN [2], Lun CHENG [2], Peter TOET [2], Ed DOPPENBERG [2], Wim DE JONG [2], Sebastian CHRUSCICKI [1]

[1] Bundesanstalt für Materialforschung und –prüfung (BAM), Berlin, Germany

[2] TNO, Delft, Netherlands

Contact e-mail: aleksander.wosniok@bam.de

ABSTRACT: In the present study, the impact of static traffic loading on the slight deflection effects in the concrete structure of an existing bridge has been investigated using distributed fiber optic sensors. In the face of increasing traffic density and severe traffic loading, the results of the load tests on the Amsterdam bridge 705 make an important contribution to the understanding of its structural behavior. The concept of the static loading was based on the use of two 36-ton trucks stopped on the bridge at multiple pre-determined locations. The load applied in this way led to location-dependent small deflection effects recorded as longitudinal strain of the sensing fiber embedded at the underside of the bridge. The measurements were performed with a commercially-available solution based on Tunable Wavelength Coherent Optical Time Domain Reflectometry with the measurement accuracy in the range of 0.5 µm/m.

1 INTRODUCTION

The continually rising volume of traffic with more often present heavy vehicles facilitates the progressive deterioration of the concrete structure of existing bridges much faster than ever before. Such deleterious effects are further accelerated by aging infrastructure often built decades ago and sometimes even approaching their service life. In view of limiting economic factors, the responsible authorities are perpetually prospecting for new cost-effective maintenance solutions targeting at a significant extension of the lifetime of the available infrastructure. The distributed fiber optic measurement methods presented in this paper are thereby an interesting alternative for assessment of structural integrity and safety evaluation of existing concrete bridges. The findings obtained during static load tests on the Amsterdam bridge 705 contribute to understanding of its structural behavior. The bridge 705 is a reinforced concrete viaduct for tram and car traffic brought into operation in 1962. The investigation of the constructional substance of this bridge is not only interesting due to the aging effects pushed on by increasing traffic associated with the urban development. As a result of the undergone remodeling and expansion of the traffic volume by an additional tram line, important structural alterations had been conducted already in an early phase of the commissioning of the bridge. For this reason, large holes had to be drilled into the newly built viaduct to construct the stairs to the intended tram stops as described by Kiers (1974). Thus, it is also the impact of the structural changes that makes the bridge so attractive for metrological investigation.

The fiber optic measurements are focused on the detection of slight deflection effects caused by two 36-ton trucks located on the bridge at multiple pre-determined locations. Furthermore, the sensing fiber measures the captured load-related deflection events as a minuscule local

longitudinal strain along the fiber glued into the small groove at the underside of the concrete bridge. This paper presents strain profiles at different positions of two trucks recorded using a high-precision distributed fiber optic sensor system based on Tunable Wavelength Coherent Optical Time Domain Reflectometry (TW-COTDR) described by Kishida (2012). The performed measurements are an important part of a complex sensor concept which involves further available and innovative technologies for static and dynamic bridge monitoring. Finally, the data evaluated here will be used to support and verify finite element models of the bridge 705 in the future. The strain measurement results can be used to calibrate a finite element calculation model serving to generate an efficient numerical model of the current as well as the prognosticated traffic volume. The utilization of measurement and monitoring data should improve an extensive model combining detailed finite element calculations with probabilistic methods for condition assessment and safety evaluation which has been developed in the framework of a 4-year research program named ERP Structural Integrity – use case concrete bridges.

2 FIBER OPTIC SENSORS FOR BRIDGE MONITORING

Distributed fiber optic sensors provide a possibility of gapless structural health monitoring (SHM) using a single standard optical fiber. The high resistance to moisture and corrosion of optical fibers as well as their small diameters and potential for long-term monitoring make the fiber optic sensor technology especially interesting for challenging tasks of bridge monitoring applications. The measurement method used here and described in 3 has crucial advantages over the traditional laser-optical deflection measurements based on conventional laser scanning approaches. Apart from the measurement range of several kilometers (up to even 25 km) and the high accuracy in the µm/m strain range, the fiber optic method applied here facilitates a long-term monitoring using the sensors implemented into the bridge structure. In contrast to the permanently installed fiber optic sensors, the typical laser scanning approaches are only suitable for short-term measuring projects, limited by the disturbing traffic under the bridge.

2.1 Sensor configuration

In the initial phase of the presented monitoring project the fiber optic sensors were installed at the underside of the bridge 705 (see Fig. 1). After notch milling, a 93.9 m section of a bare standard Corning SMF-28 Ultra optical fiber was bonded in small steps along and across the bridge deck by use of epoxy adhesive. The preliminary tests showed that such kind of sensor integration provides aligned strain transfer behavior facilitating highly sensitive strain measurements. The exact course of the bonded sensing fiber is depicted in Fig. 2. The sensor installation works were completed by connecting fiber optic pigtails leading the sensing fiber in one piece to the measurement container. The sensing fiber course shown in Fig. 2 features three 3.3 m long fiber sectors in which the fiber is triply laid (see detail 1 and 2). The sectorwise tripling of the fiber length serves the purpose of improving the spatial resolution of possible local strain events occurring in the three selected fiber sectors.

Figure 1. Underside of the bridge (left) with the integrated sensing fiber (right).

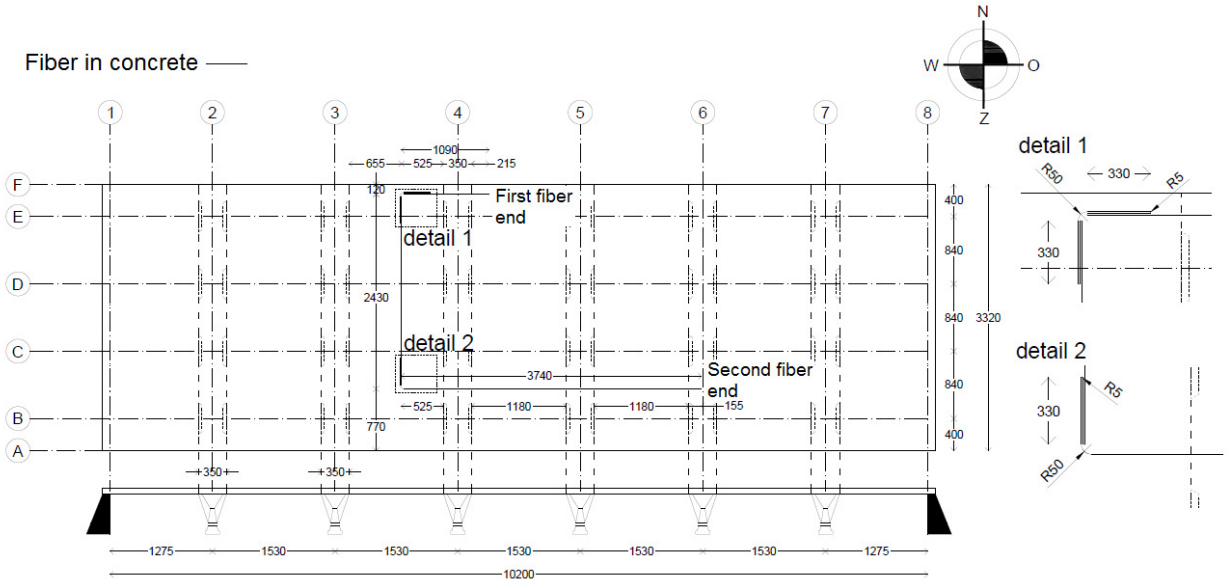

Figure 2. Course of the sensing fiber glued into the small groove at the underside of the bridge (Lengths and radiuses in centimeters).

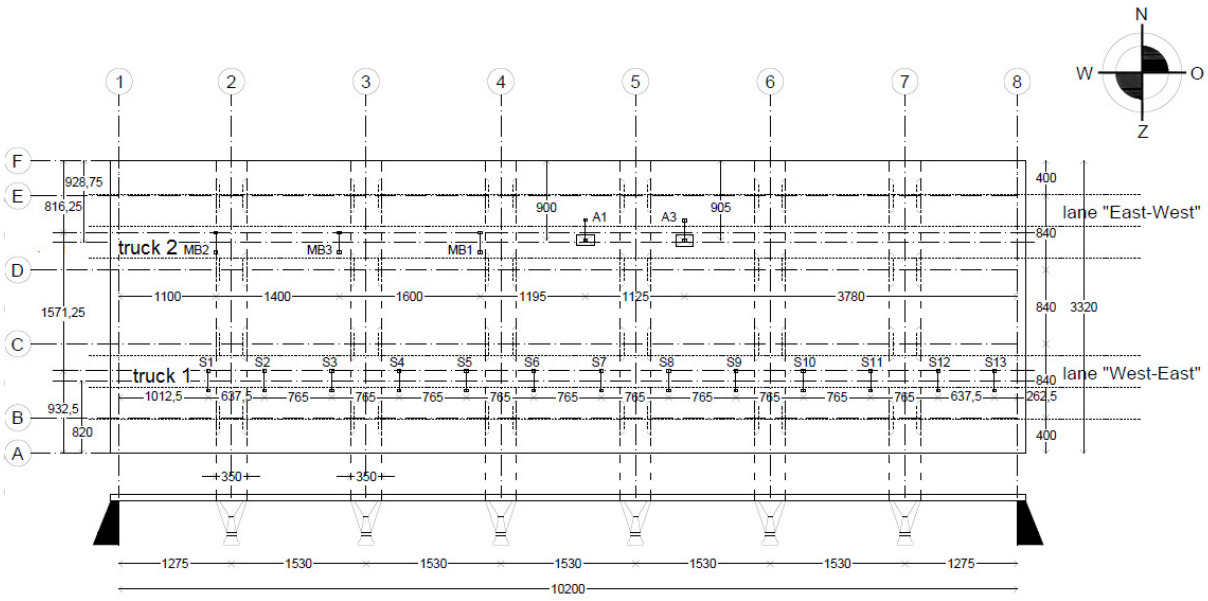

Figure 3. Positions of the two trucks during the static load tests (Lengths in centimeters).

2.2 Static loading concept

The fiber optic static measurements were performed in four measurement series by punctual loading the bridge deck using two 36-ton trucks pursuant to locations marked in Fig. 3. During all the measurement series the truck 1 was stopped at multiple locations on the bridge - at midspan of each of the spans between the columns and right above each column (positions S1 to S13). Beginning from the second measurement series, the bridge deck was additionally loaded also by a second truck (truck 2 in Fig. 3). Thereby, in the three times repeated measurement series the truck 2 remained unchanged at locations MB1 to MB3.

3 DISTRIUBUTED FIBER OPTIC SENSING METHODS

All distributed measurements during the static load tests were performed using a commercial unit NBX-7021 based on a hybrid Brillouin- and Rayleigh-based sensing technology presented by Kishida et al (2012). The hybrid device consists of both a Brillouin sensing subsystem and a Rayleigh-based TW-COTDR setup that can be selectively switched between. The separate use of one of the two measurement system configurations provides an absolute measurement of the characteristic Brillouin frequency shift ϑ_B and a relative measurement of a frequency shift $\Delta\vartheta_R$ in Rayleigh scattered optical signals, respectively. Furthermore, ϑ_B and $\Delta\vartheta_R$ depend linearly on the temperature and strain changes finally giving combined information about temperature and strain distribution along the whole sensing fiber. Since Rayleigh scattering signals are three orders of magnitude higher than those of Brillouin, the highest measurement accuracies can be achieved using Rayleigh-based approaches. However, here the determination of the measured variables is carried out relatively, i.e. by comparing two frequency-dependent intensity profiles of the Rayleigh scattering signals measured along the sensing fiber. Since only minuscule strain levels were expected during the static load tests, all the measurement series were carried out using the Rayleigh-based device configuration allowing high accuracies in the range of 0.5 µm/m. The corresponding measurement principle TW-COTDR is described in 3.2.

The measuring campaign described in this work took place after the integration of the sensing fiber at the underside of the bridge had been finished. This means that the check of slight local tensile stress induced in the sensing fiber by bonding process could have been performed only as an absolute strain measurement using distributed Brillouin fiber sensing.

3.1 Distributed Brillouin measurements

The Brillouin sensing techniques belong to the most widely established fiber optic methods for distributed strain and temperature measurement. The commercially available devices use the well-known approaches for determination of ϑ_B both in the time and frequency domain reviewed in Soto (2019) and Wosniok (2019), respectively. Generally, the Brillouin sensing systems can be operated either as a reflectometer or as a Brillouin analysis setup. The latter provides higher measurement accuracies but requires, however, connection to the both fiber ends. Such a loop configuration is therefore not feasible for every application.

Regardless of the design configuration, the Brillouin-based sensing is based on the determination of ϑ_B along the sensing fiber expressed as:

$$\vartheta_B = \vartheta_{B0} + C_B^T \cdot (T - T_0) + C_B^\varepsilon \cdot \varepsilon \tag{1}$$

where C_B^T and C_B^ε stand for the Brillouin temperature and strain coefficients, respectively. The value ϑ_{B0} is referred to the fiber-specific natural Brillouin frequency shift of an unstrained fiber at a reference temperature T_0. With a known value of ϑ_{B0}, a Brillouin frequency shift measurement allows direct conclusions about the strain-temperature conditions along the sensing fiber.

3.2 Tunable Wavelength Coherent Optical Time Domain Reflectometry

In the TW-COTDR method a tunable laser diode is used to generate power spectrum of the Rayleigh backscattered light as a function of the performed frequency scan. The frequency shift $\Delta\vartheta_R$ giving information about strain and temperature changes can be finally calculated by comparing two measurement via cross-correlation. Furthermore, comparing frequency-dependent intensity profiles of recorded Rayleigh traces with the one in reference state, the frequency shift $\Delta\vartheta_R$ to be cross-correlated varies linearly with the induced strain and temperature gradients:

$$\Delta\vartheta_R = C_R^T \cdot \Delta T + C_R^\varepsilon \cdot \Delta\varepsilon \tag{2}$$

where C_R^T and C_R^ε stand for the Rayleigh temperature and strain coefficients, respectively.

However, the highly sensitive TW-COTDR method with typical measurement times in the range of a few minutes is relatively slow. Depending on the application, a trade-off between measurement time and accuracy must be made by suited setting of the frequency step in the frequency scanning process used to obtain Rayleigh power spectra.

4 STATIC LOAD TESTS

The tests were performed according to the concept described in 2.2 in the night of Tuesday October 23 to Wednesday October 24 after the last tram crossing over the bridge to ensure an undisturbed test process.

4.1 Condition check along the whole fiber route

The bonding of the fiber into the small groove at the underside of the bridge may be associated with local strain applied to the sensing fiber. The inspection whether the sensor installation did not cause any critical strains was carried out using the single-end access configuration called Brillouin Optical Time Domain Reflectometry (BOTDR). The distribution of ϑ_B measured along the whole fiber route is illustrated in Fig. 4. The segments on the left of point A and on the right of point D correspond to the fiber optic pigtail cables. They are thus not relevant for the consideration. The Brillouin frequency shift of the single-mode bare SMF-28® Ultra fiber used as the distributed sensor can be found in the segment AD. The higher values of ϑ_B compared with those of pigtail cables indicates another fiber doping than in case of cabled fiber. The differences in the fiber doping levels generally lead to deviations in the natural Brillouin frequency shift ϑ_{B0}. Furthermore, the segments AB and CD correspond to locations where the SMF-28® Ultra fiber was coiled strain-free and placed at the underside of the bridge. The sensing relevant segment BC shows installation-related local fluctuations of measured ϑ_B along the sensing fiber bonded into the small groove for the best possible load transmission into the fiber during the static tests. As shown in Fig. 4 the bonding process caused local fiber compression (decrease of measured ϑ_B) and strain (increase of measured ϑ_B) not exceeding 15 MHz. This results in uncritical strain values up to 300 µm/m.

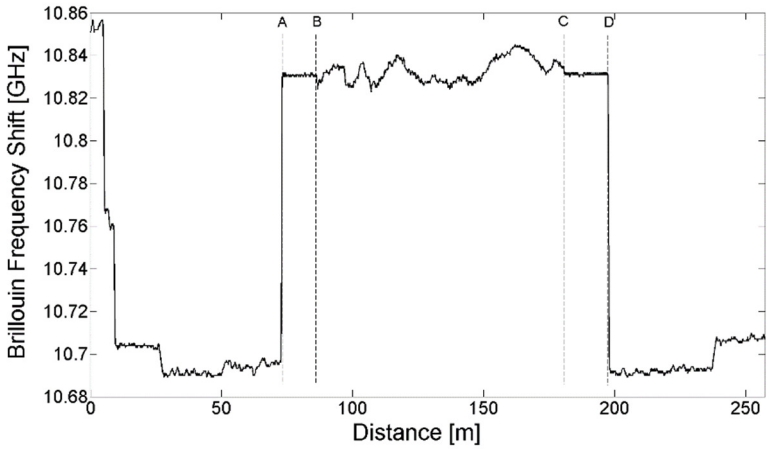

Figure 4. BOTDR measurement along the whole fiber section recorded with a spatial resolution of 50 cm and a sampling interval (distance between consecutive measuring points) of 10 cm. BC: sensing relevant section – Corning® SMF-28® Ultra fiber glued into the small groove. AB and CD: strain-free Corning® SMF-28® Ultra pigtails.

4.2 Results and analyses

The results of the static load tests are presented in detail below. Fig. 5 and Fig. 6 show all four complete measurement series. Both figures are suited for analysis of load impact of the truck 2 under the aspects of measurement repeatability. For the sake of the clarity, the load impact of the truck 1 is depicted in Fig.7-10 at separate load points generated by the weight of the truck 1.

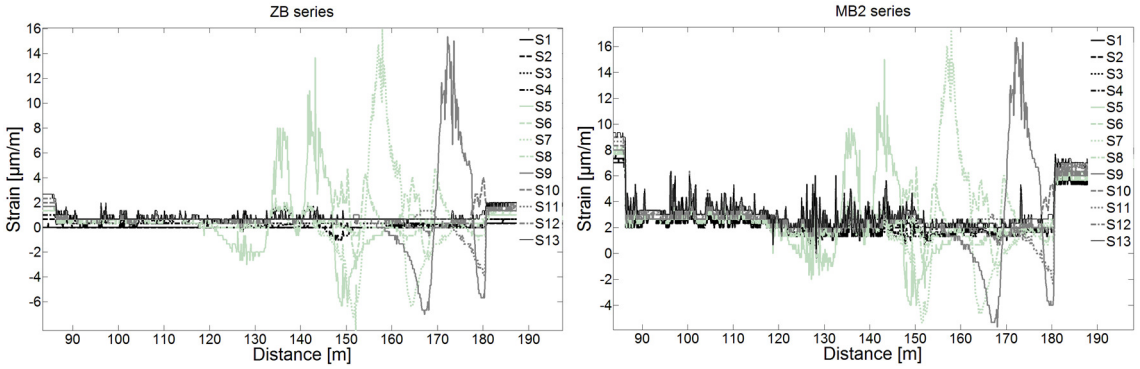

Figure 5. ZB measurement series – truck 1 passes through the positions S1 to S13, truck 2 not in use (left); MB2 measurement series – truck 1 passes through the positions S1 to S13, truck 2 at the position MB2 (right).

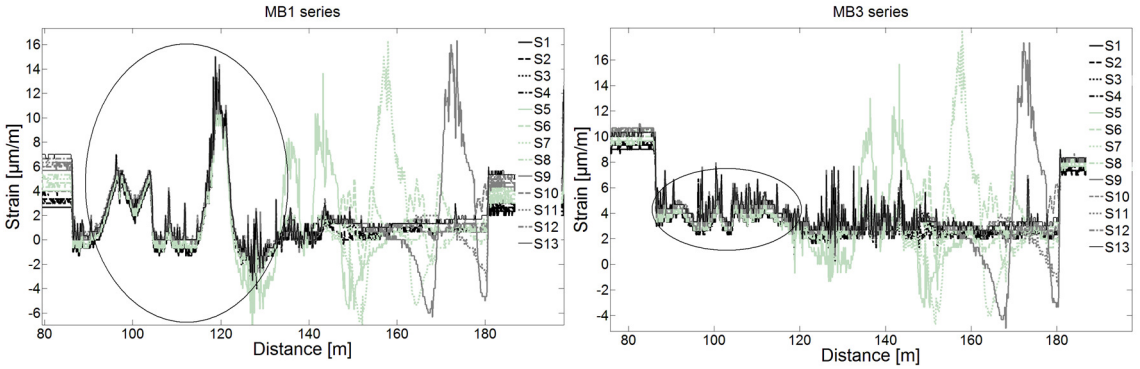

Figure 6. MB1 measurement series – truck 1 passes through the positions S1 to S13, truck 2 at the position MB1 (left); MB3 measurement series – truck 1 passes through the positions S1 to S13, truck 2 at the position MB3 (right).

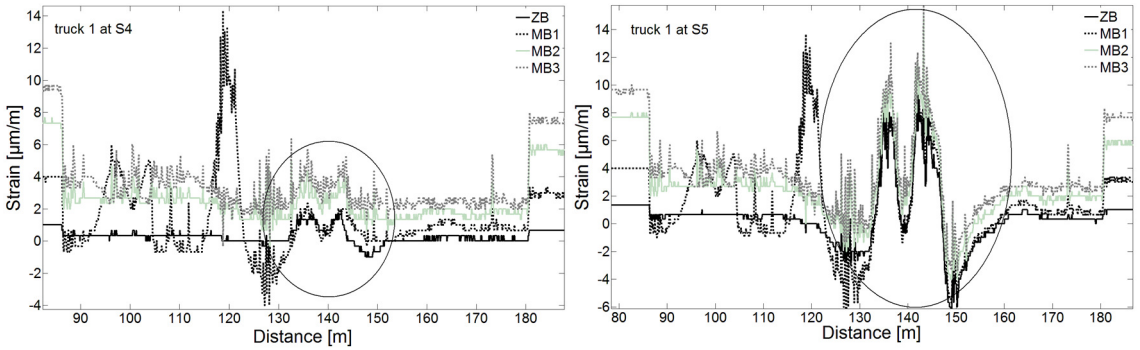

Figure 7. Strain profiles over all measurement series with the truck 1 at the position S4 (left) and S5 (right).

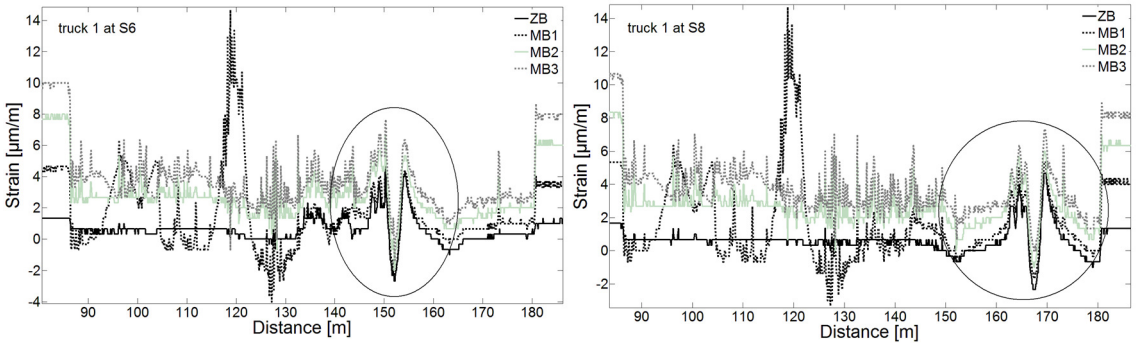

Figure 8. Strain profiles over all measurement series with the truck 1 at the position S6 (left) and S8 (right).

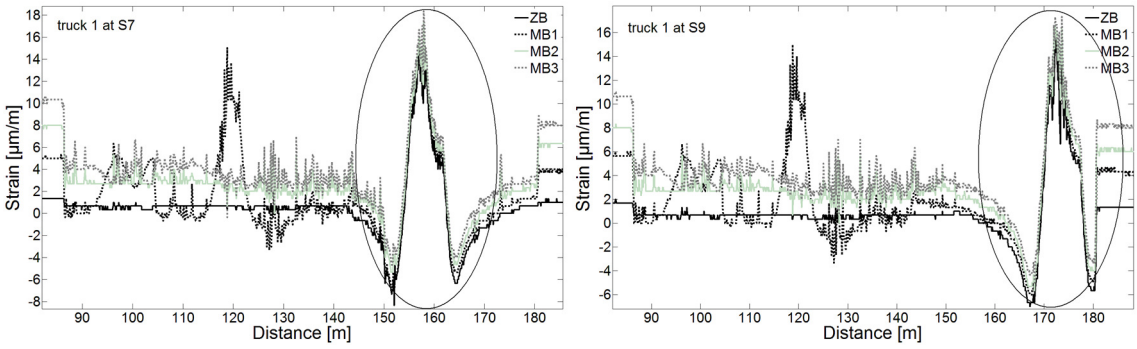

Figure 9. Strain profiles over all measurement series with the truck 1 at the position S7 (left) and S9 (right).

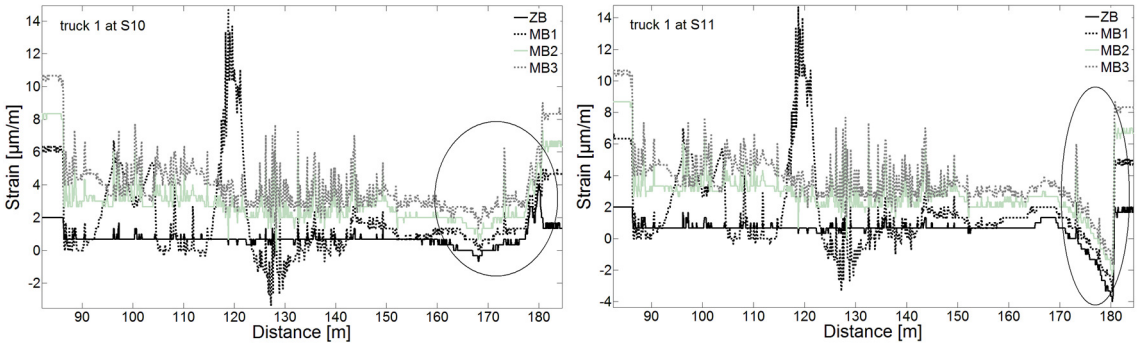

Figure 10. Strain profiles over all measurement series with the truck 1 at the position S10 (left) and S11 (right).

According to the positions of the load points generated by the weight of the truck 2 sketched in Fig. 3, the deflection effects should be detectable in the form of local longitudinal strain of the sensing fiber in the section between 86.5 m (location of the first end of the bonded sensing fiber as shown in Fig. 2) and about 125 m. Fig. 5 (right) proves that no load impact of truck 2 located in MB2 could be detected. In this case, the signal fluctuations with sharp peaks in the relevant section between 86.5 - 125 m are not directly expendable by signal noise, but rather by irreversible residual local strain induced during the duration of the static load tests. This assumption is simply confirmed by the fact that such signal fluctuations have not been measured in the coiled strain-free fiber segments AB and CD (see Fig. 4). Moreover, from the signal offset both in AB (on the left of 86.5 m in Fig. 5-10) and in CD (on the right of 180.4 m in Fig. 5-10) changes in ambient

temperature can be derived. This means that the maximum signal offset of about 10 µm/m does not represent a real strain value, but corresponds directly to a temperature change of about 1°C.

As shown in Fig. 6, the load impact of truck 2 could be detected at the location MB 1 and MB 3. In the latter case, the pointwise static load led to small strain values in the range up to 2 µm/m in the triply laid fiber sectors (see detail 1 in Fig. 2). These small strain values can be assigned to the wavy signal shape in the circled area of Fig. 6 (right). In contrast, the highest peak in the circled area of Fig. 6 (left) corresponds to the local strain of the sensing fiber integrated across the bridge below the tripled fiber sectors in detail 1.

The position-related load impact of truck 1 on the sensing fiber is presented in the circled areas of Fig. 7-10 for S4 to S11. The static load at S1 to S3, S12 and S13 has not resulted in any signal change along the fiber. By comparing diagrams in Fig. 8 and Fig. 9 conclusions about differences in the strain profiles depending on the relative position of the load points to the bridge columns can be drawn. The load rejection caused by the columns leads to reduction of local strain values at both comparable locations S6 and S8 to about 5 µm/m contrary to about 15 µm/m at S7 and S9. The strained locations S7 and S9 are additionally accompanied by significant surrounding events of compression in the range up to 7 µm/m. The circled areas in Fig. 10 show the rising edge of the comparable local strain events presented in Fig. 8 (location S10) as well as the depression edge in Fig. 9 (location S11). According to the drawing in Fig. 3 and under aspects of the exerted static load, the load impact of the location S5 should be similar to S7 and S9. Since S5 loads directly the tripled fiber sectors in detail 2 placed across the bridge, the recorded strain distribution at S5 differs from those recorded at S7 and S9.

5 CONCLUSIONS

The achieved results demonstrate the capability of the applied fiber optic system and method to detect minuscule elastic strain in the range down to about 2 µm/m at the spatial resolution of 20 cm along the 93.9-m long section of the sensing fiber. The results prove slight deflection effects depending on the location of the static load. The measurements also confirm the relief function of bridge columns for load rejection. The measurement performance allows conclusions to be drawn about the irreversible residual strain along the sensing fiber caused by the various loading steps.

6 REFERENCES

Kiers, PH., and JH. Stork, 1974. *De geschiedenis van de Amsterdamse elektrische tramlijnen*, Rotterdam, Wyt

Kishida, K., CH. Li, K. Nishiguchi, Y. Yamauchi, A. Guzik, and T. Tsuda, 2012, Hybrid Brillouin-Rayleigh distributed sensing system, *Proc. of SPIE*, 8421, 84212G-1 - 84212G-4

Soto, MA., 2019, Distributed Brillouin Sensing: Time-Domain Techniques, *Handbook of Optical Fibers*, Springer Singapore

Wosniok, A., 2019, Distributed Brillouin Sensing: Frequency-Domain Techniques, *Handbook of Optical Fibers*, Springer Singapore.